Eur. Phys. J. Appl. Phys. **33**, 51–57 (2006)
DOI: 10.1051/epjap:2005088

THE EUROPEAN PHYSICAL JOURNAL APPLIED PHYSICS

Noise and response characterization of an anisotropic magnetoresistive sensor working in a high-frequency flipping regime

A. Bertoldi[1], L. Botti[2], D. Covi[3], R. Buffa[2], D. Bassi[1], and L. Ricci[1,a]

[1] Dipartimento di Fisica, Università di Trento, 38050 Trento-Povo, Italy
[2] Dipartimento di Fisica, Università di Siena, 53100 Siena, Italy
[3] NeuriCam S.p.A., Via S. Maria Maddalena, 12, 38100 Trento, Italy

Received: 12 February 2005 / Received in final form: 2 August 2005 / Accepted: 29 September 2005
Published online: 6 December 2005 –

Abstract. We report on the characterization of the behaviour of an anisotropic magnetoresistive sensor undergoing a 100 kHz flipping of the magnetic domains, i.e. at frequencies two/three orders of magnitude higher than conventionally recommended. The noise analysis allows for the optimal setting of the relevant parameters defining such high-frequency, and hitherto unexplored, operation regime. Precision and accuracy performance in static conditions have been assessed by keeping into account the role of the sensor temperature. This last parameter has been evaluated by suitably manipulating the signals occurring at the sensor itself. The used technique can provide the base for a temperature sensor conditioning to be employed in magnetometers using this kind of devices.

PACS. 07.07.Df Sensors (chemical, optical, electrical, movement, gas, etc.); remote sensing – 73.43.Qt Magnetoresistance – 85.70.Kh Magnetic thin film devices: magnetic heads (magnetoresistive, inductive, etc.); domain-motion devices, etc.

1 Introduction

Among the several kinds of magnetic field sensors [1], anisotropic magnetoresistive (AMR) devices [2] have become widely used because of their peculiar properties. Standard AMR sensors [3] have size slightly larger than 1 mm, measurement bandwidth covering the interval from zero to several MHz and measurement range from less than 1 nT to 1 mT. An integrated AMR probe is usually available in form of a Wheatstone bridge formed by four AMR thin film elements. If the bridge is supplied at two opposite terminals, a voltage difference occurs at the remaining terminals. Such voltage is proportional both to the supply voltage and the component of the magnetic field along a given direction. The order of magnitude of sensitivity is typically 10 mV V^{-1} mT^{-1}.

The existence of an imbalance between the resistance values of the bridge elements makes up the main drawback related to the use of these sensors. This imbalance generates an output zero-field offset voltage that is typically equivalent to a field strength of the order of 0.1 mT. Both zero-field offset voltage and sensitivity are temperature-dependent, with fractional temperature coefficients of the order of $10^{-3}\,K^{-1}$. Consequently, absolute measurements of the field strength are severely hampered.

The problem deriving by the zero-field offset voltage can be overcome by exploiting the following property: if the magnetization of the AMR film domains is flipped, the bridge response to the applied field changes sign, whereas the zero-field offset voltage remains unchanged. This quantity can be therefore cancelled out by subtracting two readouts measured under opposite film magnetizations [4]. The film magnetization flipping is achievable by means of a suitably strong saturating field. On many commercially available devices, this field is generated by sending a suitable current pulse through an additional integrated conducting strap (*set/reset strap*); a pulse duration of at least 1 μs is usually required. Such devices allow for the implementation of a periodic offset cancellation procedure. A typical cycle is characterized by the generation of a magnetization current pulse, the measurement of the resulting AMR bridge output voltage, the generation of a second magnetization current pulse (opposite to the former one), the measurement of the new AMR bridge output, and finally the calculation of the difference between the two readouts. All these operations are time-consuming: in order to maximize the measurement bandwidth of a system implementing such procedure, it is crucial to minimize the duration of each single step.

[a] e-mail: ricci@science.unitn.it

Table 1. Main characteristics of the Honeywell HMC1021 AMR sensor [7].

dynamic range	± 0.6 mT
sensitivity	10 mV V^{-1} mT^{-1}
bandwidth	5 MHz
noise density	48 nV/Hz$^{1/2}$ @ 1 Hz, $V_{bridge} = 5$ V
	4.2 nV/Hz$^{1/2}$ @ 1 kHz
bridge resistance	1100 Ω
dimensions	$4.9 \times 3.9 \times 1.5$ mm^3

In this paper we present the analysis of the behaviour of a commercially available AMR sensor subject to a flipping frequency of 100 kHz. This frequency is two/three orders of magnitude higher than usually declared by constructors [5,6]. The noise characterization allows to determine the optimal operation regime regarding the timing and the flipping current pulses at such high flipping frequencies. The static response of the sensor, i.e. the assessment of precision and accuracy, has been carried out by considering the effects of the sensor temperature. This parameter has been extrapolated by measuring the resistance of the integrated set/reset strap. Such technique could be employed for implementing a temperature sensor conditioning and thus improving the performance of conventional AMR magnetometers. The used AMR sensor is HMC1021 [7] by Honeywell. The method described is applicable to other sensors of the same kind.

The paper is organized as follows: the measurement setup and timing are described in Section 2; the noise characterization is described and discussed in Section 3; finally, Section 4 regards the static response.

2 Measurement setup and timing

Table 1 shows the main characteristics of the used device. The sensing elements of the AMR bridge are made of permalloy thin films. The sensor has an on-chip set/reset strap, magnetically-coupled to the AMR film domains and allowing for their magnetization. The magnetic field strength is measured in a single direction; henceforth, the term *magnetic field* and the related values will refer to the component along the sensing direction.

The measurement setup and timing are schematically shown in Figures 1 and 2, respectively. The set/reset strap is placed in the middle of a so-called MOSFET H-bridge, supplied by a stable current source. The set and reset current pulses through the strap are generated by closing two of four MOSFETs. The pulse duration T_p is fixed to 1 μs. After a set pulse, the output of the AMR bridge V_{bridge} is given by

$$V_{bridge}(S) = V_{offset} + \frac{1}{2} S \cdot V_{supply} \cdot B,$$

where S is the sensitivity, B the magnetic field strength, V_{offset} the zero-field offset voltage and V_{supply} the supply

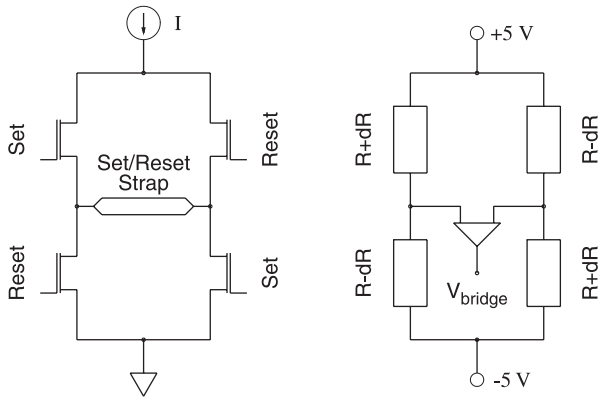

Fig. 1. Essential schematics of the measurement setup. The left side shows the set/reset strap placed in the middle of the external MOSFET H-bridge. The right side shows the AMR bridge and the instrumentation amplifier connected at its output. The resistance variation is proportional to the magnetic field applied to the sensor.

voltage. After a reset pulse, one has

$$V_{bridge}(R) = V_{offset} - \frac{1}{2} S \cdot V_{supply} \cdot B.$$

The bridge output V_{bridge} is amplified by an instrumentation amplifier (gain $G = 100$) and then sampled by a 16-bit resolution analog-to-digital converter (ADC). The AMR bridge voltage supply (± 5 V) and the ADC analog input voltage range (± 10 V) are chosen to optimize the readout resolution of the nominal dynamic range of the sensor (± 0.6 mT). The ADC output is sent to an external digital unit. This module, which communicates with a personal computer (PC), drives the magnetization current pulses, triggers the analog-to-digital acquisition and carries out the difference of the readouts acquired under opposite magnetizations. In this way, an offset-free, field-proportional numerical value $\tilde{B}_{out}$ is yielded:

$$\tilde{B}_{out} = \frac{2^{16}\ \text{LSB}}{20\ \text{V}}\ G\ V_{out},$$

where V_{out} is defined as

$$V_{out} \equiv V_{bridge}(S) - V_{bridge}(R) = S \cdot V_{supply} \cdot B.$$

In the last expression, $V_{bridge}(S)$ and $V_{bridge}(R)$ are assumed to correspond to two consecutive samplings. The entire sequence has a period T of 20 μs. Since an acquisition is carried out every $T/2 = 10$ μs, a magnetic field value is provided at the rate of 100 kHz. Beyond the digital value corresponding to V_{out}, the setup also provides an analog signal corresponding to the voltage drop V_{SR} across the set/reset strap (resistance $\approx$ 8 Ω). For this purpose, an instrumentation amplifier having unitary gain and -3 dB bandwidth of 6 MHz is used. The quantity V_{SR} has been used to monitor the temperature of the sensor, as explained in Section 4.

The AMR probe and all the circuitry necessary to get a numerical, field-dependent output, as well as additional

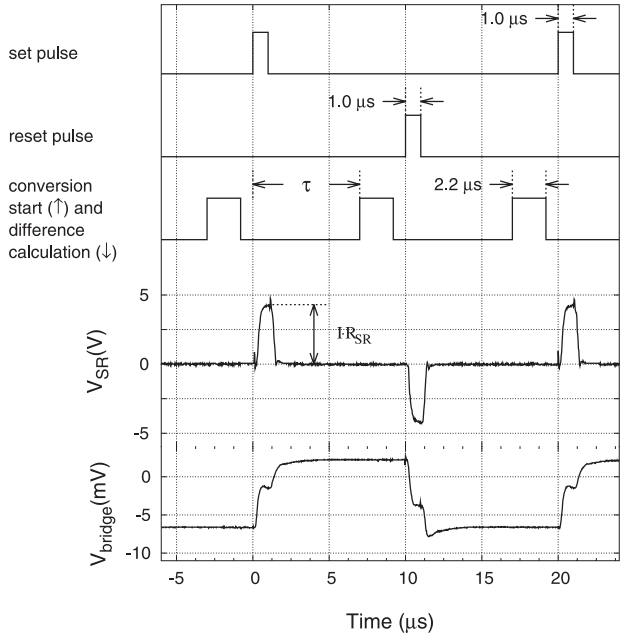

Fig. 2. Timing scheme of the setup operation. The trace above corresponds to the digital, 1 μs long signal which closes the MOSFET pair of the H-bridge so as to generate the positive (set) magnetization current pulses. Analogously, the second trace corresponds to the signal which drives the negative (reset) magnetization current pulses. The relative delay between the two pulse trains is 10 μs. The third trace corresponds to the pulse triggering, at the rising edge, the ADC conversion-start and, at the falling edge, the difference calculation. The whole acquisition and processing phase requires 2.2 μs. The next waveform shows the output of the instrumentation amplifier with unitary gain monitoring the voltage drop across the set/reset strap. The last waveform corresponds to the signal at the output of the instrumentation amplifier with gain 100 connected with the AMR bridge. In this figure, $I = 0.5$ A and $\tau = 7$ μs.

components for the power supply and the I/O operations, are mounted on a rectangular printed circuit board of size 70×53 mm^2. The relevant analog waveforms propagate over distances of less than 40 mm. A more detailed description of the measurement setup and the external unit goes beyond the goal of the present paper and is the subject of reference [8], focussed on the development of a high-performance magnetometer.

All measurements described in the following sections have been carried out by real-time processing the digital output and using a single sensor. Many measurements have been repeated on two other sensors of the same kind, showing the same behaviour. The output voltage V_{out}, rather than the numerical value $\tilde{B}_{out}$, is used in the following for the discussion of the sensor characterization.

3 Noise characterization

Besides flipping frequency and pulse duration, the two main parameters which characterize the operation of an AMR sensor in a continuous flipping regime are (see Fig. 2) the time τ elapsing between the start of a current pulse and the following ADC conversion-start trigger signal, and the magnetization pulse current I. This last quantity is more precisely defined as an average value:

$$I \equiv \frac{1}{2\,T_p} \int_t^{t+T} |I\,(t')|\,dt'\,, \tag{1}$$

where T and T_p are the sequence period and the pulse duration, respectively. The topic of this section is the noise density characterization of the AMR sensor output V_{out} as a function of the time τ and the pulse current I.

According to the specifications provided by the constructor [7], the $1/f$ noise component is negligible at frequencies higher than a few hundred Hz. So, as the present analysis aims to characterize the sensor behaviour at frequencies of the order of $10 \div 100$ kHz, the noise density generated by the sensor is assumed to be white. With the used measurement procedure, the $1/f$ noise is not suppressed, but rather uniformly *smeared out* over the measurement bandwidth. The output voltage noise density is evaluated by determining the root-mean-square (rms) voltage noise and the equivalent noise bandwidth of the measurement setup.

The rms voltage noise is measured as follows. A set of 256 consecutive readouts is sampled in a time of 2.56 ms and then transferred to the PC for further processing. In absence of any deterministic noise source (ex.gr. the power line at 50 Hz) the rms noise can be evaluated by taking the standard deviation of the samples around their average value. However, since deterministic noise sources (mainly the 50 Hz power line) turn out not to be negligible, a preliminary rms noise value is taken as the standard deviation of the residuals from the best-fit, third-order polynomial evaluated on the set. The polynomial order equal to 3 has been chosen as it approximates sections of sinusoid better than a parabola; moreover, an additional analysis has shown that the rms deviation is essentially independent on the polynomial order n if $n \geq 3$. The procedure is repeated 16 times, each producing an outcome; the sample mean of these outcomes and the related standard deviation are then taken as final rms noise value and its uncertainty, respectively.

The equivalent noise bandwidth of the measurement setup is mainly determined by the dynamic response of the instrumentation amplifier (nominal -3 dB bandwidth $\nu_{3\,\mathrm{dB}}$ equal to 800 kHz at $G = 100$). In order to more precisely assess the bandwidth, a series of noise measurements have been carried out by adding low-pass RC-filter stages between the instrumentation amplifier and the ADC. For these measurements, I and τ have been set to 0.5 A and 8 μs, respectively. In case of a white noise spectrum, the square rms voltage noise N^2 is expected to linearly depend on the bandwidth BW:

$$N^2 = N_o^2 + e_n^2 \cdot BW, \tag{2}$$

where N_o is the noise offset, mainly due to the ADC quantization and conversion error, and e_n is the white voltage

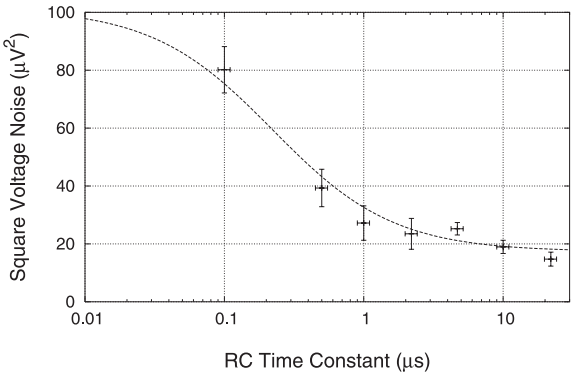

Fig. 3. Square rms voltage noise as a function of time constant RC. The bandwidth has been varied by changing the capacitance C of a low-pass filter stage placed at the output of the instrumentation amplifier. The bandwidth error has been evaluated by assigning a 10% relative precision on the product RC. Due to the logarithmic scale, the plot does not show an additional point obtained without filter ($RC = 0$, $N^2 = 99$ $[\mu\mathrm{V}]^2$). The measurements have been carried out at a magnetic field of approximately 10 μT. The reduced χ^2 resulting from the fit is 1.5.

noise spectral density. In addition:

$$BW = \left(BW_o^{-1} + 4\ RC\right)^{-1}, \tag{3}$$

where BW_o is the sought equivalent noise bandwidth and RC the time constant of the filter. Figure 3 shows the measured dependence as well as the best-fit curve obtained by combining equations (2, 3). The fit provides a noise offset N_o of 4.2(2) μV (or equivalently 1.4(1) LSB), a noise density e_n of 8.6(2) nV/Hz$^{1/2}$ and an equivalent noise bandwidth BW_o of 1.1(4) MHz. This last value is in very good agreement with the value given by the nominal dynamic response of the instrumentation amplifier ($BW = \nu_{3\,\mathrm{dB}}\ \pi/2$). Henceforth, for the determination of the output voltage noise density the value 1.1 MHz will be used as equivalent noise bandwidth of the measurement setup.

3.1 Noise as a function of time τ

The time τ affects both sensitivity and noise (see Fig. 2). The determination of the noise dependence on τ is therefore important for the assessment of the maximum flipping frequency. The measurements have been carried out for two different values of the pulse current I and by exposing the sensor to different constant field strengths. The field strength has been varied by using a permanent magnet. Figure 4 shows the results. Three significant aspects can be noticed: (i) the noise does not depend on the field strength; (ii) there is no evidence of a dependence on the pulse current I; (iii) for $\tau > 4$ μs the noise does not depend on τ. The origin of the light noise increase for time values progressively smaller than 4 μs is unclear. However, contributions arising from the MOSFET H-bridge switching speed (in combination with the inductive/resistive load of

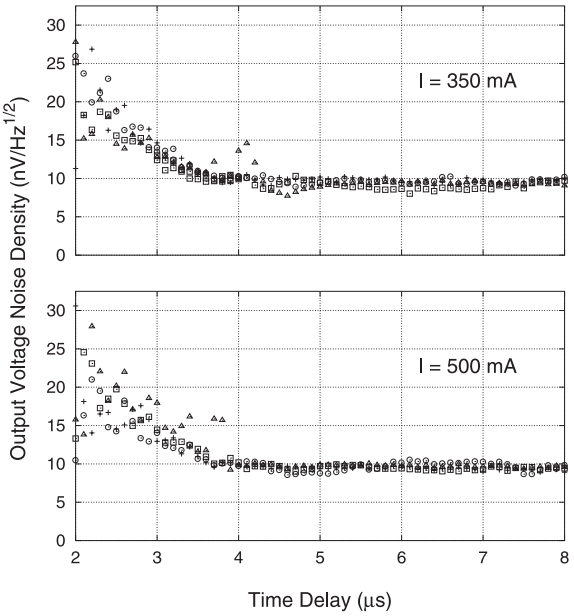

Fig. 4. Output voltage noise density as a function of time τ, for $I = 0.35$ A (above) and $I = 0.5$ A (below). In both graphs, crosses, squares and circles represent data points acquired at -260 μT, 20 μT and 280 μT, respectively. The triangles represent data acquired at approximately zero field with a second measurement head and sensor pair.

the set/reset strap) or the response time of the instrumentation amplifier following the AMR sensor can be ruled out, as it results from Figure 5. The shape of the V_{SR} signal shows that the switching time of the MOSFETs is by far smaller than 3 μs. In addition, both the voltage measured directly at the output of the AMR bridge and the output of the following instrumentation amplifier have essentially the same settling time: an evidence that the instrumentation amplifier does not introduce any significant bandwidth limitation with regard to the output of the AMR bridge.

The measurements described in this section suggest the possibility of enhancing the flipping frequency to values of $150 \div 200$ kHz or – at expense of a light noise increase – even higher. However, this would result in a higher duty and therefore an increased power dissipation and temperature of the AMR sensor, with a consequent performance degradation. With regard to the measurements discussed in the following sections, the time τ has been fixed at 8 μs.

3.2 Noise as a function of pulse current I

Figure 6 shows the dependence of the output voltage noise density on the pulse current I. The output voltage noise density shows a minimum for a pulse current I in the range $0.25 \div 0.5$ A. As expected, for smaller current values the noise rapidly increases as a consequence of an insufficient domain alignment. The output noise also shows a slightly increasing trend at higher currents. This behaviour can be accounted for by the increasing sensor temperature,

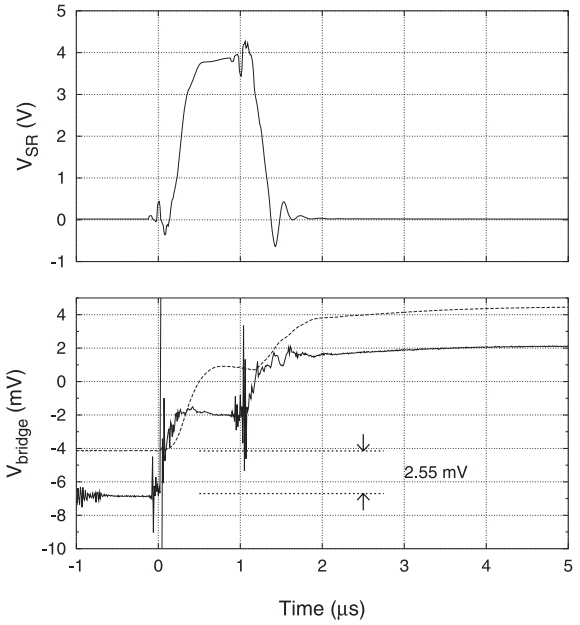

Fig. 5. Detail of the transients following a magnetization current pulse: (above) output of the instrumentation amplifier with unitary gain monitoring the voltage drop across the set/reset strap; (below) the continuous line corresponds to the AMR bridge output measured directly at the device output terminals, while the dashed line corresponds to the output of the instrumentation amplifier ($G = 100$) following the AMR sensor and rescaled by a factor 1/100. The offset of 2.55 mV between the last two signals is due to the input offset voltage of the instrumentation amplifier (this offset is also cancelled out in the difference operation). The time origin is chosen at the rising edge of the digital pulse controlling the closing of the MOSFET pair for the generation of a *set* pulse. The amplitude I of the current pulse in the set/reset strap amounts to 0.5 A. All signals have been acquired by means of a 600 MHz bandwidth oscilloscope; for the acquisition of the AMR bridge output, two 500 MHz probes have been used.

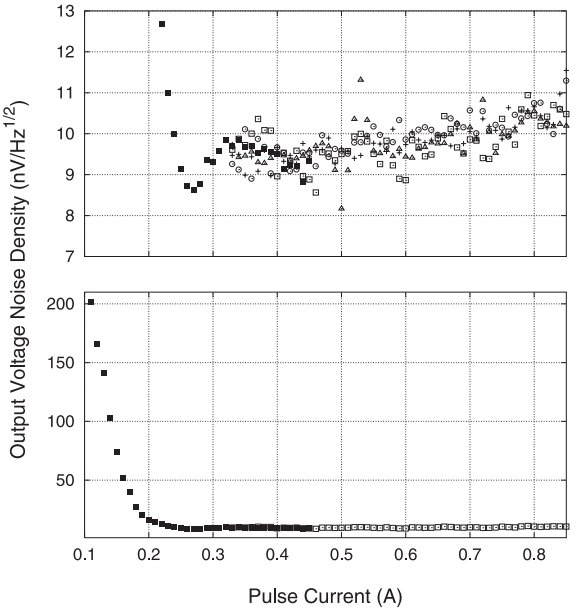

Fig. 6. Output voltage noise density as a function of the pulse current I. In the plot above, crosses, empty squares and circles represent data points acquired at -260 μT, 10 μT and 290 μT, respectively, while triangles represent data acquired at approximately zero field with a second measurement head and sensor pair. Full squares correspond to data acquired with a slightly modified version of the reference measurement head: for $I < 0.3$ A the voltage drop across the set/reset strap becomes too small and impedes the optimal operation of the MOSFET H-bridge. For this reason, and uniquely for this measurement, an additional 10 Ω SMD resistance has been connected in series with the strap at the output of the H-bridge. The plot below shows with a magnified voltage noise density scale the data acquired at approximately zero field.

which, also by virtue of a resistance increase, increases the Johnson noise contribution. Again, the noise shows no dependence on the applied magnetic field.

3.3 Noise analysis

Table 2 sums up the output voltage noise density measured with $I = 0.5$ A, at different field strength values, and both in case of enabled and disabled flipping. The no-flipping value of approximately 6 nV/Hz$^{1/2}$ is larger than the expected value of the Johnson noise density of the AMR bridge, i.e. 4.2 nV/Hz$^{1/2}$ (this value corresponds to a temperature of 20 °C and a bridge resistance of 1100 Ω). This discrepancy can be in part accounted for by the temperature – and consequently resistance – increase of the bridge AMR films: temperature measurements carried out with a temperature sensor installed in thermal contact with the sensor case revealed, in regime of disabled flipping, a temperature increase of 20 K with respect to the environment. Other noise sources are the $1/f$ noise component and the electronics generating the ±5 V reference voltage.

Under normal operation, the noise density turns out to be slightly larger (∼10%) than the value corresponding to the flipping-free operation multiplied by $\sqrt{2}$ (the normal operation output is calculated as the difference of two readouts). The small additional noise amount, which is further introduced when the set/reset pulses are sent through the strap, can be accounted for by the temperature and resistance increase of the sensor: under normal operation the sensor case temperature increases by 44 K with respect to the environment. Other possible sources are electromagnetic interferences and the MOSFET quiescent current.

4 Static response precision and accuracy

The static response of the sensor has been investigated by using the following setup. The head has been inserted within a cylindrical reference electromagnet (inner diameter 97.0 mm, length 130.2 mm), with the sensor located at its center and the sensing direction parallel to the coil

Table 2. Output voltage noise density measured at different field strengths, in case of disabled and enabled flipping. The last line refers to data measured with a second measurement head and sensor pair.

field (μT)	output voltage noise density (nV/Hz$^{1/2}$)	
	without flipping	with flipping
–290	6.4(4)	9.3(6)
10	6.2(4)	9.7(6)
290	6.3(5)	9.4(7)
10	5.1(5)	9.5(5)

axis. The field produced has been evaluated by measuring the current I_{coil} flowing in the coil. Such assessment has a relative uncertainty of 0.2%. This figure reflects the uncertainty both on the determination of the current I_{coil} and on the relative position and orientation between reference coil and sensor. The sensor is thus exposed to a field B given by the sum of a known component B_{coil}, due to the coil, and an unknown, environmental component B_o: $B = B_o + B_{coil}$. All measurements described in this section have been carried out overnight, i.e. in conditions of highest stability of the field B_o. The use of μ-metal shields in order to minimize $|B_o|$ has been ruled out mainly because it would have required a much more complicated determination of the field generated by the coil.

For a given value of B_{coil}, obtained by setting a suitable I_{coil}, the measurement system acquires two quantities: the output voltage V_{out} and the component A_{SR} at frequency $T^{-1} = 50$ kHz of the signal V_{SR} (see Fig. 2). This last measurement is carried out by means of a lock-in amplifier; in case of perfectly square pulses of amplitude modulus $\hat{V}_{SR}$, one would have $A_{SR} = (2\sqrt{2}\hat{V}_{SR}/\pi)\sin(\pi T_p/T)$, i.e. $A_{SR} \cong 0.141\ \hat{V}_{SR}$ for $T_p/T = 1/20$. As the average peak current flowing through the set/reset strap, i.e. the quantity I defined in equation (1), is kept constant by the external current source, the voltage A_{SR} provides a value proportional to the set/reset resistance and thus to the temperature of the AMR sensor (henceforth a linear relation between A_{SR} and the sensor temperature is assumed). The relevance of the evaluation of this quantity is clear from Figure 7, where data gathered at constant field but at different temperatures are shown. The data distribution is well described by a constant negative temperature coefficient of the sensitivity, in agreement with the specifications declared by the constructor.

The magnetic field has been varied within the nominal range (±0.6 mT) of the AMR sensor. The result of a typical measurement is shown in Figure 8. In order to describe the output voltage V_{out} dependence on the magnetic field B and the sensor temperature (or, equivalently, the amplitude A_{SR}), the following model function has been chosen:

$$V_{out} = (a_0 + b_0 A_{SR})\,\frac{B}{H_o}\sqrt{1 - \left(\frac{B}{H_o}\right)^2}, \qquad (4)$$

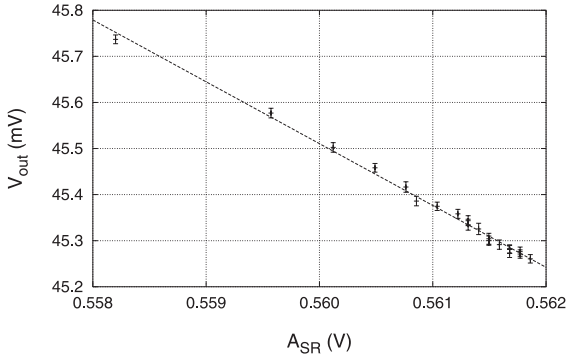

Fig. 7. Output voltage V_{out} as a function of the set/reset voltage drop amplitude A_{SR}, measured at a constant magnetic field (290 μT). Each point and the related error bar represent the sample mean and the standard deviation, respectively, calculated over a set of 256 consecutive readouts. The dashed straight-line corresponds to the best-fit straight line fitting the data.

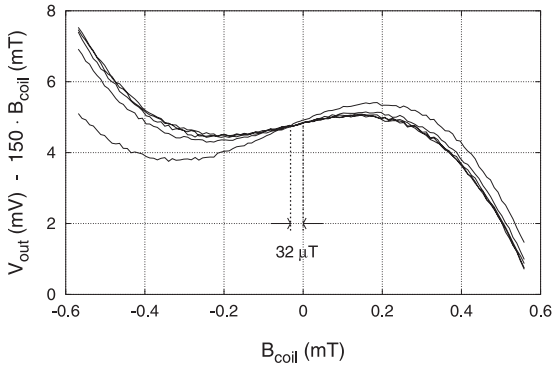

Fig. 8. Output voltage V_{out} as a function of coil field B_{coil}. The main linear dependence has been subtracted in order to highlight the non-linear contributions. For a given value of B_{coil}, the data points are distributed on different curves as a consequence of different environmental temperatures (resulting in different sensor temperatures). The curves approximately cross at a point corresponding to an environmental field B_o of +32 μT. Each data point represents the sample mean calculated over a set of 256 consecutive readouts.

where a_0, b_0 and H_0 are, together with B_0, the parameters to be determined; a_0 and H_0 have the dimension of a voltage and a magnetic field, respectively, while b_0 is dimensionless. This model corresponds to the standard response of AMR sensors realized, as in the present case, by means of the so-called barber-poles [9]. According to the plot of Figure 7, the sensitivity coefficient is assumed to be linearly dependent on the temperature ($a_0 + b_0 A_{SR}$). The model has been tested in two steps: first, the four parameters have been determined by means of a non-linear fit on a set of measured data (fit set); second, the generalization capability of the model has been verified by using other sets of measured data (test sets), as follows. Given a measured data point (B_{coil}, V_{out}, A_{SR}), let $\tilde{B}$ be the magnetic field calculated by inverting the model equation of equation (4) and using both the best-fit parameters and the measured values of V_{out} and A_{SR}. Moreover, let δ be

Table 3. Generalization capability of the model described by equation (4), both for $I = 0.35$ A and $I = 0.5$ A.

fit set	I, $\lvert B\rvert$, $\chi^2_{reduced}$	test set #	μ_δ (nT)	σ_δ (nT)
A	0.35 A	1	182	1085
	≤ 0.6 mT	2	139	1153
	11.03	3	188	1132
		4	926	839
B	0.5 A	5	5	246
	≤ 0.6 mT	6	8	293
	9.37	7	58	282
		8	39	289
B	0.5 A	5	22	129
	≤ 0.15 mT	6	3	147
	2.75	7	–23	125
		8	14	116

the residual defined as $\tilde{B} - B$. The average μ_δ and the standard deviation σ_δ of the residual δ, computed over a test set, can be then taken as estimators for the accuracy and the precision of the model, respectively. The measurements have been carried out for the pulse current values of 0.35 A and 0.5 A, i.e. approximately at the boundary of the optimal operation range for I described above. The results are shown in Table 3.

Two main aspects can be noticed: first, both μ_δ and σ_δ are smaller at higher current; second, reducing the analysis range by a factor 4 results in a further improvement of both estimators by a factor 2. In the case $I = 0.5$ A and $|B| \leq 0.15$ mT, accuracy and precision can be evaluated in about 25 nT and 100 nT, respectively. It has to be remarked that these values could be overestimated as a consequence of external (environmental) magnetic noise. Finally, the typical value of the sensor sensitivity, extrapolated by the setup parameters and by the coefficient $a_0 + b_0 A_{SR}$ of equation (4), is 7.6 mV V^{-1} mT^{-1}.

We are indebted to M. Prevedelli for useful discussions. This work has been in part supported by the INFM "Progetto di Ricerca Avanzata *Photon Matter*".

References

1. J.E. Lenz, Proc. IEEE **78**, 973 (1990)
2. S. Krongelb, J. Electron. Mater. **2**, 227 (1973)
3. W. Kwiatkowski, S. Tumanski, J. Phys. E: Sci. Instrum. **19**, 502 (1986)
4. M. Ueda, M. Endoh, H. Yoda, N. Wakatsuki, IEEE T. Magn. **26**, 1572 (1990)
5. M.J. Caruso, *Set/Reset Pulse Circuits for Magnetic Sensors*, Honeywell Application Note, AN-201
6. *Magnetic Field Sensors* (Philips Datasheet, 1998)
7. *HMC1001, HMC1002, HMC1021 and HMC1022 1 and 2-Axis Magnetic Sensors*, Honeywell Datasheet, Doc. No. 900248 Rev. B 4-00.
8. A. Bertoldi, D. Bassi, L. Ricci, D. Covi, S. Varas, Rev. Sci. Instrum. **76**, 065106 (2005)
9. U. Dibbern, IEEE T. Magn. **20**, 954 (1984)